Journal: Physical Review Research

Accession code: WM10228

Article Title: Fano resonance in excitation spectroscopy and cooling of an optically trapped single atom

First Author: Chang Hoong Chow

AUTHOR QUERIES - TO BE ANSWERED BY THE CORRESPONDING AUTHOR

The following queries have arisen during the typesetting of your manuscript. Please answer these queries by marking the required corrections at the appropriate point in the text.

1	Please check inserted page number.
2	Please check author provided DOI information.

Important Notice to Authors

Attached is a PDF proof of your forthcoming article in Physical Review Research. Your article has 8 pages and the Accession Code is **WM10228**.
Your paper will be in the following section of the journal: RESEARCH ARTICLES

Please note that as part of the production process, APS converts all articles, regardless of their original source, into standardized XML that in turn is used to create the PDF and online versions of the article as well as to populate third-party systems such as Portico, Crossref, and Web of Science. We share our authors' high expectations for the fidelity of the conversion into XML and for the accuracy and appearance of the final, formatted PDF. This process works exceptionally well for the vast majority of articles; however, please check carefully all key elements of your PDF proof, particularly any equations or tables.

Figures submitted electronically as separate files containing color appear in color in the journal.

No further publication processing will occur until we receive your response to this proof.

ORCIDs

Please follow any ORCID links ( ) after the authors' names and verify that they point to the appropriate record for each author. Requests to add ORCIDs should be sent no later than the first proof revisions. If authors do not subsequently add/authenticate ORCIDs within seven business days, production of the paper will proceed and no further requests to add ORCIDs will be processed. See complete details regarding ORCID requests and ORCID verification at https://journals.aps.org/authors/adding-orcids-during-proof-corrections.

NOTE: If this paper is an Erratum or a Reply, the corresponding author's ORCID may be present if previously provided to APS, but no ORCIDs can be added at proof stage.

Crossref Funder Registry ID

Information about an article's funding sources is now submitted to Crossref to help you comply with current or future funding agency mandates. Crossref's Funder Registry (https://www.crossref.org/services/funder-registry/) is the definitive registry of funding agencies. Please ensure that your acknowledgments include all sources of funding for your article following any requirements of your funding sources. Where possible, please include grant and award ids. Please carefully check the following funder information we have already extracted from your article and ensure its accuracy and completeness:

- National Research Foundation, NRF2021-QEP2-01-P01/W21Qpd0101

Other Items to Check

- Please note that the original manuscript has been converted to XML prior to the creation of the PDF proof, as described above. Please carefully check all key elements of the paper, particularly the equations and tabular data.
- Title: Please check; be mindful that the title may have been changed during the peer-review process.
- Author list: Please make sure all authors are presented, in the appropriate order, and that all names are spelled correctly.
- Please make sure you have inserted a byline footnote containing the email address for the corresponding author, if desired. Please note that this is not inserted automatically by this journal.
- Affiliations: Please check to be sure the institution names are spelled correctly and attributed to the appropriate author(s).
- Receipt date: Please confirm accuracy.
- Acknowledgments: Please be sure to appropriately acknowledge all funding sources.
- Hyphenation: Please note hyphens may have been inserted in word pairs that function as adjectives when they occur before a noun, as in "x-ray diffraction," "4-mm-long gas cell," and "*R*-matrix theory." However, hyphens are deleted from word pairs when they are not used as adjectives before nouns, as in "emission by x rays," "was 4 mm in length," and "the *R* matrix is tested."

  Note also that Physical Review follows U.S. English guidelines in that hyphens are not used after prefixes or before suffixes: superresolution, quasiequilibrium, nanoprecipitates, resonancelike, clockwise.
- Please check that your figures are accurate and sized properly. Make sure all labeling is sufficiently legible. Figure quality in this proof is representative of the quality to be used in the online journal. To achieve manageable file size for online delivery, some compression and downsampling of figures may have occurred. Fine details may have become somewhat fuzzy,

especially in color figures. Figures to be published in color online will appear in color on these proofs if viewed on a color monitor or printed on a color printer.

- Please check to ensure that reference titles are given as appropriate.
- Overall, please proofread the entire *formatted* article very carefully. The redlined PDF should be used as a guide to see changes that were made during copyediting. However, note that some changes to math and/or layout may not be indicated.

Ways to Respond

- Web: If you accessed this proof online, follow the instructions on the web page to submit corrections.
- Email: Send corrections to prrproofs@aptaracorp.com
  Subject: **WM10228** proof corrections

PHYSICAL REVIEW RESEARCH **00**, 003000 (2024)

Fano resonance in excitation spectroscopy and cooling of an optically trapped single atom

Chang Hoong Chow [1], Boon Long Ng [1], Vindhiya Prakash [1], and Christian Kurtsiefer [1,2,*]

[1] *Center for Quantum Technologies, 3 Science Drive 2, Singapore 117543*

[2] *Department of Physics, National University of Singapore, 2 Science Drive 3, Singapore 117542*

(Received 12 December 2023; accepted 22 February 2024; published xxxxxxxxxx)

Electromagnetically induced transparency (EIT) can be used to cool an atom in a harmonic potential close to the ground state by addressing several vibrational modes simultaneously. Previous experimental efforts focus on trapped ions and neutral atoms in a standing wave trap. In this work, we demonstrate EIT cooling of an optically trapped single neutral atom, where the trap frequencies are an order of magnitude smaller than in an ion trap and a standing wave trap. We resolve the Fano resonance feature in fluorescence excitation spectra and the corresponding cooling profile in temperature measurements. A final temperature of around 6 μK is achieved with EIT cooling, a factor of 2 lower than the previous value obtained using polarization gradient cooling.

DOI: 10.1103/PhysRevResearch.00.003000

I. INTRODUCTION

Single neutral atoms in optical dipole traps form a potential basis for quantum information processing applications, including quantum simulation [1,2], computation [3,4], and communication [5,6]. Ideally, the atom can be prepared in an arbitrary quantum state and can be made to exchange quantum information coherently with a tightly focused optical mode. A prerequisite for an efficient coupling between a photon and an atom is minimizing the atomic position uncertainty, which requires the atom to be sufficiently cooled [7]. Furthermore, cooling of the atom can extend the coherence time of the qubit state [4,8,9] and allow for the manifestation of quantum mechanical properties of the atomic motion [10,11]. A lower atomic temperature can also improve the fidelity of one- and two-qubit gates, which is useful for the implementation of quantum computers and analog quantum simulators [12–14].

Raman sideband cooling techniques [15–17] can be employed to cool atoms to the motional ground state of the trapping potential. However, this method requires an iteration of the cooling process over several laser settings to address individual vibrational modes. Alternatively, cooling by electromagnetically induced transparency (EIT) is a simpler approach that can also help achieve ground state cooling.

EIT cooling relies on suppression of diffusion when a three-level atom is transferred to a superposition of the ground states that is decoupled from the excited state (dark state). On probing the excitation spectrum of a Λ system with a strong field (coupler) and a weaker probe, the dark state is revealed via a reduction in fluorescence when the probe and coupler are equally detuned from the excited state. This dip, in combination with the fluorescence peak from the dressed state, results in an asymmetric Fano profile [18]. When the motional spread of the atomic wave packet in an external conservative potential is taken into account, the dark state becomes sensitive to the atomic position. Particularly, cooling occurs when the dark state is decoupled from the excited state at the carrier frequency but is coupled to the bright (dressed) state at the red sideband [19]. For this, the system simply needs to be engineered such that frequency difference between the dark state and the bright dressed state matches the vibrational mode spacing of the potential (see Fig. 1).

It is worth mentioning that gray molasses cooling is another sub-Doppler cooling technique that relies on the suppressed scattering from a dark state in a three-level system [20–23]. However, this scheme requires three counterpropagating and phase-stable pairs of probe and coupling beams directed at the atom along the three coordinate axes as cooling is achieved through a Sisyphus mechanism of the atom traversing rising and falling potentials [20]. While it may be well suited for cold clouds of high phase-space density, the EIT cooling technique presented here is a simpler alternative for single atoms as it requires only a pair of intersecting light fields.

The Fano profile was first observed in the fluorescence spectroscopy of a single barium ion [24,25], and a cooling technique exploiting this effect was proposed 15 years later [26]. Since then, this EIT cooling method has been implemented in platforms such as trapped ions [27–29], neutral atoms confined in standing wave traps [30], and quantum gas microscopy setups [31].

In this work, we investigate free-space EIT cooling of a single neutral ^{87}Rb atom in a mK deep far-off-resonant optical dipole trap (FORT), where the trap frequencies are typically around tens of kHz, one to two orders of magnitude smaller than in typical standing wave traps and ion traps. A three-level Λ system is realized using the magnetic sublevels in the hyperfine manifolds of the ground and excited states. We first

*christian.kurtsiefer@gmail.com

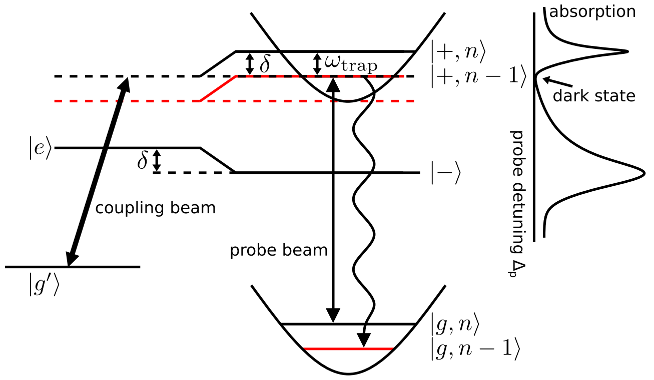

FIG. 1. Left: EIT cooling transition in a three-level Λ system. A strong coupling beam forms new eigenstates $|+\rangle$ and $|-\rangle$ from the bare atomic states $|g'\rangle$ and $|e\rangle$. Here n denotes the vibrational quantum number for atomic motion in a harmonic trap with a frequency of ω_{trap}. By choosing a suitable intensity for the coupling beam, the scattering spectrum can be engineered such that the transition $|g,n\rangle \rightarrow |+,n-1\rangle$ is enhanced to achieve cooling. Right: spectral profile of the dressed states. Scattering of a weak probe beam that couples an atom prepared in ground state $|g\rangle$ to the dressed states reveals two peaks corresponding to each of the dressed states and an asymmetric-Fano profile due to the dark state.

resolve the Fano profile via excitation spectroscopy and then implement a cooling scheme on altering the configuration and detunings. We also explore the parameter space to identify detunings and intensities that minimize the temperature.

II. THEORETICAL OVERVIEW

Theoretical descriptions of the Fano spectrum and cooling by EIT have been extensively reported earlier [18,19,25,26]. Here we summarize the results and extend some of the outcomes to describe our measurements. Consider a Λ system formed by two ground states $|g\rangle$ and $|g'\rangle$ as well as an excited state $|e\rangle$ that can decay to both ground states with a total decay rate Γ. A weak (strong) probe (coupling) field of frequency ω_p (ω_c) couples $|g\rangle$ ($|g'\rangle$) to $|e\rangle$ with a Rabi frequency Ω_p (Ω_c) and a detuning $\Delta_p = \omega_p - \omega_{eg}$ ($\Delta_c = \omega_c - \omega_{eg'}$).

In the limit of a weak probe driving field ($\Omega_p \ll \Omega_c, \Delta_c$), the ground state $|g\rangle$ remains an eigenstate with the eigenvalue $\lambda_g = (\Delta_c - \Delta_p)$. The other two eigenstates $|\pm\rangle$ are associated with the two light-shifted resonances close to $\Delta_p = 0$ and $\Delta_p = \Delta_c$ as the probe detuning Δ_p is being varied. Their corresponding eigenvalues are $\lambda_+ = -\delta - i\Gamma_+/2$ and $\lambda_- = \Delta_c + \delta - i\Gamma_-/2$, respectively, with an associated light shift δ and radiative decays $\Gamma_\pm$ [25]. For a large detuning $\Delta_c \gg \Omega_c, \Gamma$, these can be obtained through a perturbative expansion of $1/\Delta_c$:

$$\delta = \frac{\Omega_c^2}{4\Delta_c},$$
$$\Gamma_+ = \Gamma\frac{\Omega_c^2}{4\Delta_c^2},$$
$$\Gamma_- = \Gamma - \Gamma_+ = \Gamma\left(1 - \frac{\Omega_c^2}{4\Delta_c^2}\right). \tag{1}$$

For a larger Ω_p, the probe-induced coupling between $|g\rangle$ and $|e\rangle$ cannot be neglected and the light shifts and decay rates have been obtained from the steady-state solution for the three-level optical Bloch equation in the vicinity of $\Delta_p = \Delta_c$ [25]:

$$\delta = \frac{\Delta_c}{4\Delta_c^2 + \Gamma^2}\left(\Omega_c^2 - \Omega_p^2\right),$$
$$\Gamma_+ = \frac{\Gamma}{4\Delta_c^2 + \Gamma^2}\left(\Omega_c^2 + \Omega_p^2\right). \tag{2}$$

The narrow resonance associated with λ_+ is shown to exhibit a Fano-shaped profile [18] and possess a spectral width $\Gamma_+ \ll \Gamma$ for $\Omega_c, \Omega_p \ll \Delta_c$. The Fano-type profile manifests in the excitation spectrum of the scattering rate $|T|^2$ [18]:

$$|T|^2 \propto \frac{[2\delta/\Gamma_+ + 2(\Delta_p - \Delta_c - \delta)/\Gamma_+]^2}{1 + [2(\Delta_p - \Delta_c - \delta)/\Gamma_+]^2}, \tag{3}$$

which matches the form of a typical Fano profile [32].

When including the atomic center-of-mass motion of the atom to the description, the energy change due to recoil from a scattering event should be considered. For an atom confined in a harmonic potential of frequency ω_{trap}, when the position uncertainty is much smaller than the wavelength of light (Lamb-Dicke limit), the coupling between the motional states and internal energy levels is characterized by the Lamb-Dicke parameter $\eta = |\vec{k}_p - \vec{k}_c| \cos(\phi)\, a_0$. Here $\vec{k}_p$ and $\vec{k}_c$ are the wave vectors of the probe and coupling beams, ϕ is the angle between $\vec{k}_p - \vec{k}_c$ and the motional axis, and $a_0 = [\hbar/(2m\omega_{\text{trap}})]^{1/2}$ is the position uncertainty of the particle with mass m in the ground state of the harmonic oscillator [26]. For an atom initially in the dark internal state and the motional eigenstate $|n\rangle$, the momentum imparted by light when $|\vec{k}_p - \vec{k}_c| \neq 0$ leads to coupling with the bright state $|+\rangle$ of neighboring motional modes $|n \pm 1\rangle$. By choosing $\Delta_p = \Delta_c > 0$ and a suitable Ω_c such that $\delta = \omega_{\text{trap}}$, the scattering spectrum can be tailored such that the transition probability of the $|g,n\rangle \rightarrow |+,n-1\rangle$ red sideband transition is greater than the probability of the $|g,n\rangle \rightarrow |+,n+1\rangle$ blue sideband transition. This results in effective cooling. A detailed quantitative analysis of the cooling dynamics using a rate equation description is provided in [19,26].

III. FANO SPECTRUM

To observe the Fano spectrum from a single ^{87}Rb atom, we consider a Λ system formed by the Zeeman sublevels $|g\rangle \equiv |F=2, m_F=-2\rangle$ and $|g'\rangle \equiv |F=2, m_F=0\rangle$ of the $5\,^2S_{1/2}$ F=2 hyperfine ground state and $|e\rangle \equiv |F'=3, m_{F'}=-1\rangle$ of the $5\,^2P_{3/2}$ F'=3 excited state, subject to a pair of laser beams with opposite polarizations [see Fig. 2(a)]. A stronger left circularly polarized (σ^-) coupling beam of Rabi frequency Ω_c couples $|g'\rangle$ to $|e\rangle$ with a detuning Δ_c. A weaker right circularly polarized (σ^+) probe beam of Rabi frequency Ω_p and detuning Δ_p drives the $|g\rangle \leftrightarrow |e\rangle$ transition.

Figure 2(b) shows a schematic of our experimental setup. We trap a single ^{87}Rb atom at the focus of a pair of high numerical-aperture (NA = 0.75) aspheric lenses in a far-off-resonant dipole trap (FORT). The FORT is formed by a linearly polarized Gaussian laser beam at 851 nm, tightly

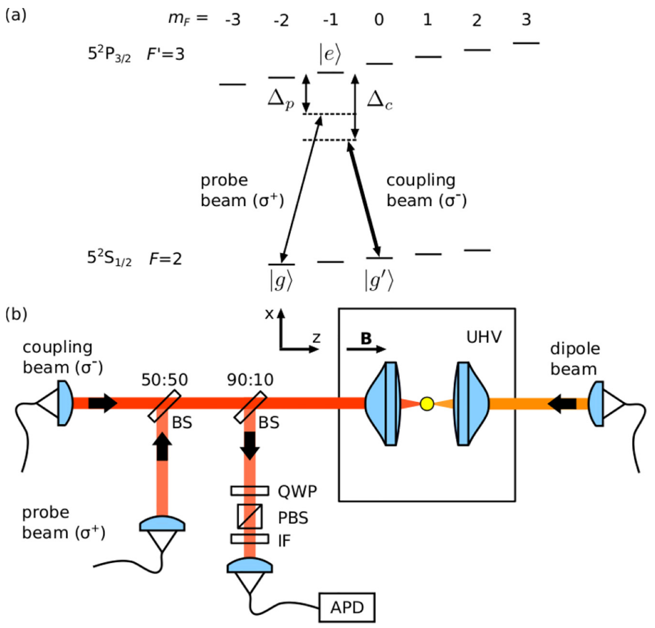

FIG. 2. (a) Energy levels and transitions in ^{87}Rb used for observing the Fano scattering profile. (b) Experimental configuration for Fano spectroscopy. The backscattered atomic fluorescence is collected by a high numerical aperture lens and coupled to a single-mode fiber connected to an avalanche photodetector. BS: beam splitter; QWP: quarter-wave plate; PBS: polarizing beam splitter; IF: interference filter; APD: avalanche photodetector; UHV: ultrahigh vacuum; B : magnetic field.

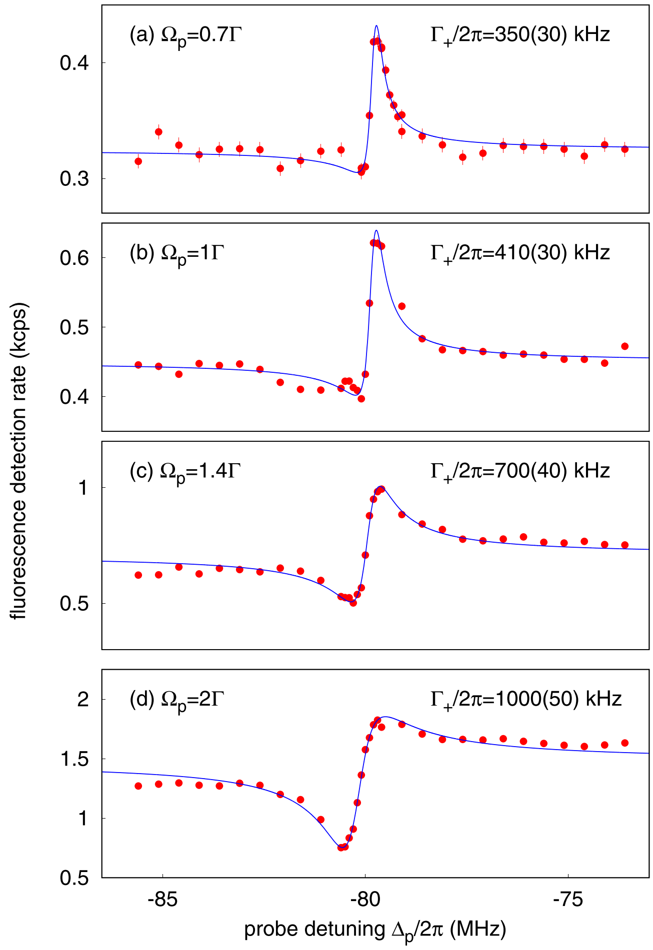

FIG. 3. Observation of Fano scattering profiles. Red dots: single photon scattering detected in APDs from the two-photon process for $\Delta_c/2\pi = -80$ MHz and $\Omega_c = 1.4\Gamma$, projected into the probe polarization. Blue curve: fits to Fano profiles following Eq. (3). The probe beam power increases from subplot (a) to (d) as indicated by the Rabi frequency values. All plots show a clear suppression in scattering around $\Delta_p/2\pi = -80$ MHz, where the atom is optically pumped to the dark state. Error bars represent one standard deviation due to propagated Poissonian counting statistics.

focused to a waist of $w_0 = 1.1$ μm. The aspheric lenses not only enable tight spatial confinement of the atom in the FORT, but also allow efficient collection of fluorescence from the atom. Refer to [33] for a complete description of our single atom trap.

For driving the Λ system, the coupling and probe beams employed are generated from the same external cavity diode laser. This ensures a fixed phase relationship between the two driving fields. The light from this laser is split into two paths for the coupling and probe beams with the frequency of light independently controlled by an acousto-optic modulator (AOM) in each path. The two beams are then overlapped in a beam splitter (BS) and copropagate to the atom in this part of the experiment. The copropagating configuration minimizes the momentum transfer to the atom ($\Delta\vec{k} = \vec{k}_c - \vec{k}_p = 0$ and, equivalently, $\eta = 0$) via the two-photon process, thereby decoupling the center-of-mass motion from the dynamics and allowing the Fano profile to be resolved.

To prevent probe and coupling beams from entering the detection system, the atomic fluorescence is collected in the backward direction using a 90:10 BS. An interference filter (IF) prevents dipole trap radiation from reaching the detectors. Additionally, we employ a polarization filter consisting of a quarter-wave plate (QWP) and a polarizing beam splitter (PBS) to eliminate scattering from the $|F = 2, m_F = -2\rangle \to |F' = 3, m_{F'} = -3\rangle$ cycling transition induced by the strong coupling field.

When a single ^{87}Rb atom is loaded into the FORT, we apply 10 ms of polarization gradient cooling (PGC) to cool the atom to a temperature of 14.7(2) μK, as measured by the "release-recapture" technique [34,35]. Then, a bias magnetic field of 1.44 mT is applied along the FORT laser propagation direction to remove the degeneracy of the Zeeman states. Next, the single atom is illuminated with the pair of strong coupling and weak probe beams for 3 ms. During this interval, the atomic fluorescence is detected using an avalanche photodetector (APD). The measurement is repeated for approximately 3000 runs for various values of Ω_p as Δ_p is tuned across a range of $\pm 2\pi \times 6$ MHz centered at Δ_c. The coupling beam parameters remain fixed at $\Delta_c = -2\pi \times 80$ MHz and $\Omega_c = 1.4\Gamma$.

Figure 3 shows a series of scattering spectra for increasing probe powers. The detected photoevents shown here also include the APD's dark counts, which contribute to a background of around 300 events per second. Red points are experimental data and blue lines are fits to Eq. (3).

In all measurements, an asymmetrical Fano peak is observed with a linewidth smaller than the natural linewidth ($\Gamma = 2\pi \times 6$ MHz). The asymmetry of the Fano profiles can be characterized by the Fano parameter q, given by $q = 2\delta/\Gamma_+$ in our system [18,32]. The Fano parameters q extracted from the fits are all positive, indicating that the profiles are right skewed, with a decreasing q for increasing probe power [$q = 2.4(2)$, 2.0(1), 1.21(6), and 0.72(3) for probe Rabi frequencies of $\Omega_p = 0.7\Gamma$, Γ, 1.4Γ, and 2Γ, respectively].

The Fano linewidths extracted from the fits increase linearly with the probe power [$\Gamma_+/2\pi = 350$ (30), 410 (30), 700 (40), and 1000 (50) kHz for saturation parameters of $2\Omega_p^2/\Gamma^2 = 1,\ 2,\ 4,$ and 8, respectively]. Compared to the theoretical predictions from Eq. (2) (yielding $\Gamma_+/2\pi \approx 83$, 100, 132, and 201 kHz), the measured values are larger by a factor of 4.7(6). This discrepancy could be attributed to the presence of multiple Fano resonances resulting from other Zeeman sublevels. Specifically, there is a Λ configuration formed by the states $|F = 2, m_F = -1\rangle$, $|F' = 3, m_{F'} = 0\rangle$, and $|F = 2, m_F = 1\rangle$, as well as another Λ configuration formed by the states $|F = 2, m_F = 0\rangle$ ($|g'\rangle$), $|F' = 3, m_{F'} = 1\rangle$, and $|F = 2, m_F = 2\rangle$. The coupling strengths are quite different for these Λ configurations, which leads to distinct values for shifts and linewidths in the Fano resonances. Consequently, the scattering profiles for these three sets of Λ configurations would overlap and distort the total scattering rate, causing the apparent broadening in the excitation spectrum (refer to the Appendix A for more discussion).

Furthermore, the energy of the dark state indicated by the dip in the scattering spectra should ideally remain fixed at $\Delta_p = \Delta_c = 2\pi \times -80$ MHz, independent of the Rabi frequencies Ω_c and Ω_p of the driving fields. However, we observe that the minimum of the scattering spectra shifts to a larger detuning for increasing Ω_p. It seems likely that this is because the probe field Ω_p also drives the transition between the state $|g'\rangle = |F = 2, m_F = 0\rangle$ and the excited state $|F' = 3, m_{F'} = 1\rangle$, which is not taken into account in the three-level model. This coupling introduces an additional light shift on the $|g'\rangle$ state, leading to a shift in the scattering spectrum for increasing probe field strength.

IV. COOLING OF ATOMIC MOTION

Having developed a better understanding of the absorption profile, we now turn to the cooling of atomic motion. In order to utilize the sensitivity of the internal dark state to the spatial gradient of the electric fields, we require a configuration in which the momentum transferred by light to the atom is nonzero ($\Delta\vec{k} = \vec{k}_c - \vec{k}_p \neq 0$). For this, the direction of the probe beam is altered such that it is sent orthogonal to the coupling beam in a top down direction, polarized parallel to the bias magnetic field to excite π transitions (see Fig 4). The Λ configuration is now realized with a σ^- polarized coupling light connecting the $|g'\rangle \equiv |F = 2, m_F = -1\rangle$ sublevel of the $5\,^2S_{1/2}$ $F = 2$ hyperfine ground state and the $|e\rangle \equiv |F' = 2, m_{F'} = -2\rangle$ sublevel of the $5\,^2P_{3/2}$ $F' = 2$ hyperfine excited state, and a π polarized probe light connecting sublevel $|g\rangle \equiv |F = 2, m_F = -2\rangle$ of the $5\,^2S_{1/2}$ $F = 2$ hyperfine ground state to $|e\rangle$. Both coupling and probe are blue-detuned from their respective transitions by

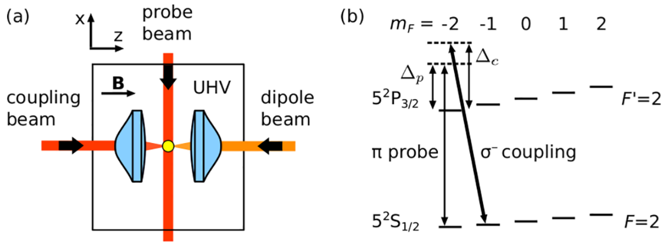

FIG. 4. (a) Experimental configuration for the off-resonant EIT cooling process. The probe beam propagates orthogonally to the optical axis to allow for motional coupling. (b) Energy levels and transitions in ^{87}Rb used in the cooling experiment.

$\Delta_c = \Delta_p = 2\pi \times 94.5$ MHz $\approx 16\Gamma$. With this detuning, we are able to satisfy the condition of forming a narrow Fano resonance that preferentially drives the red motional sideband transition, as described in the last paragraph of Sec. II.

Our FORT traps the atom in a 3D harmonic oscillator with radial ($\omega_{x/y}$) and axial (ω_z) trapping frequencies $(\omega_{x/y}, \omega_z) = 2\pi \times [73(2), 10(1)]$ kHz, deduced from a parametric excitation measurement [36]. Accordingly, the associated Lamb-Dicke parameters (η_x, η_z), which quantify the motional coupling, are estimated to be (0.23, 0.61) for our EIT cooling beam geometry.

Similar to the experimental sequence described in the previous part, we start with 10 ms of PGC to cool the atom upon successful loading, followed by a bias magnetic field of 1.44 mT along the FORT laser propagation direction to remove the degeneracy of the Zeeman states. We then apply EIT cooling on the Λ system by switching on the coupling beam and probe beam for 20 ms, a duration chosen to be sufficiently long to ensure that the system reaches a steady state. During this cooling process, a weak repumper beam resonant to the $D1$ line at 795 nm between $5\,^2S_{1/2}$ $F = 1$ and $5\,^2P_{1/2}$ $F' = 2$ is also switched on to transfer the atom back into the $F = 2$ hyperfine ground state if it spontaneously decays into the $F = 1$.

Following that, we employ a "release and recapture" method [34,35] to quantify the temperature of the single atoms. During this process, the EIT cooling beams are switched off and the atom is released from the trap for an interval τ_r by switching off the FORT beam. Subsequently, the FORT is switched on to recapture the atom and we observe atomic fluorescence by switching on the MOT's cooling and repumping beams to check the presence of the single atom. We repeat each experiment around 200 times to obtain an estimate of the recapture probability. We then infer the atomic temperature by comparing the experimentally obtained recapture probability at τ_r to Monte Carlo simulations of recapture probabilities for single atoms at various temperatures [34].

In the first part of the thermometric experiment, we investigate the capability of the two-photon process to either cool down or heat up the single atoms. We apply EIT cooling by varying Δ_p and Δ_c over a range of $\pm 2\pi \times 1$ MHz while fixing Ω_c and Ω_p to $2\pi \times 5.2$ MHz and $2\pi \times 2.0$ MHz, respectively. We choose $\Omega_c = 2\pi \times 5.2$ MHz because this parameter is expected to give a Fano resonance shift coinciding with the

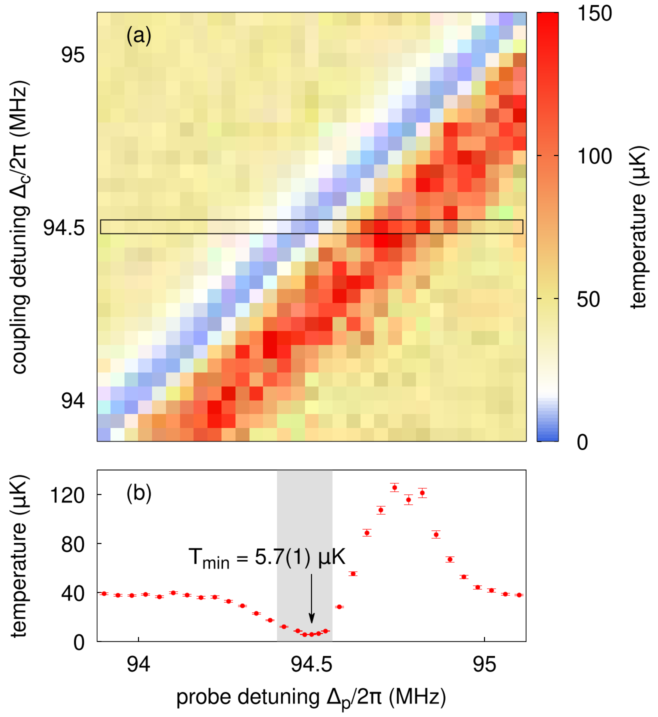

FIG. 5. (a) Atomic temperature for various probe and coupling field detunings, inferred from release and recapture measurements after 20 ms of EIT cooling. The antidiagonal blue band indicates dark state resonance, which has the highest cooling efficiency. (b) EIT cooling profile in atomic temperature as a function of probe detuning Δ_p for a fixed coupling detuning [here $\Delta_c = 2\pi \times 94.5$ MHz as indicated by the boxed region in (a)] also shows an asymmetric Fano feature. The area shaded in gray represents the range of probe detunings where an effective cooling is observed.

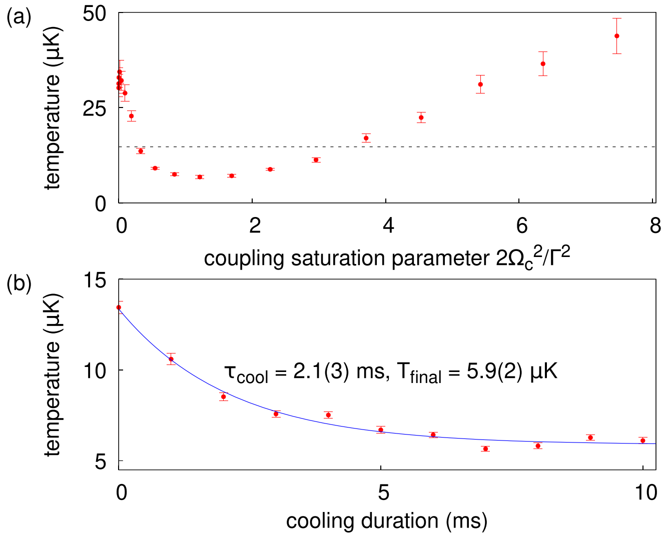

FIG. 6. (a) Atomic temperature at $\Delta_p = \Delta_c = 2\pi \times 94.5$ MHz for varying Ω_c. We observe an effective cooling for $s = 2\Omega_c^2/\Gamma^2$ between 0.5 and 3, with the optimal cooling around $s = 1.42(3)$ (cooling duration fixed to 20 ms). The dotted line indicates the initial atomic temperature after PGC of 14.7 μK. Error bars represent standard error of binomial statistics accumulated from around 200 repeated runs. (b) Atomic temperature measured after different cooling durations. A cooling time of 2.1(3) ms and final temperature of 5.9(2) μK are extracted from the exponential fit.

trap frequency [$\delta = \omega_{x/y}$ following Eq. (1)] that leads to optimal cooling. Here, we fix the release interval to $\tau_r = 30$ μs, empirically determined to yield the largest signal contrast for recapturing measurements from which the temperature can be inferred.

The resulting atomic temperature is shown in Fig. 5(a). Cooling and heating effects close to the dressed states for the two-photon process are significantly visible. We observe an effective cooling in the antidiagonal stripe where $\Delta_p = \Delta_c$, in agreement with the theoretical prediction. Heating occurs most dominantly around $\Delta_p = \Delta_c + 2\pi \times 250$ kHz, where the blue sideband transitions have a larger probability. For frequencies far away from the Fano resonance, the single atom undergoes incoherent scatterings of the pump and probe beams. In this process, the atom experiences recoil heating which raises the atomic temperature to about 40 μK.

In the following parts, we maintain Δ_c to be fixed at $2\pi \times 94.5$ MHz. To obtain a more accurate estimation of the atomic temperature, we now deduce a temperature value based on a series of recapturing probabilities for 12 different release intervals, ranging from 1 to 80 μs. We vary the probe detuning Δ_p around Δ_c, as shown in Fig. 5(b). We observe the typical asymmetric Fano profile also in the temperature of the atoms, with the lowest temperature of 5.7(1) μK measured at $\Delta_p = \Delta_c$.

We expect optimal cooling to be achieved when the dressed state energy shift δ caused by the coupling beam is equal to the trap frequency, $\delta = \omega_{x/y}$, as it maximizes the absorption probability on the red sideband transition [19]. To confirm this behavior, we record the atomic temperature using the same "release and recapture" scheme for different coupling beam powers, keeping $\Delta_c = \Delta_p = 2\pi \times 94.5$ MHz and $\Omega_p = 2\pi \times 2.0$ MHz fixed. The results are shown as a function of the saturation parameter $s = 2\Omega_c^2/\Gamma^2$ in Fig. 6(a). Cooling is observed for s between 0.5 and 3, with the lowest temperature obtained at an optimal cooling parameter of $s = 1.42(3)$ [or $\Omega_c = 2\pi \times 5.06(5)$ MHz]. This corresponds to a dressed state energy shift of $\delta = \Omega_c^2/(4\Delta_c) \approx 2\pi \times 68(1)$ kHz, as introduced in Eq. (2), which is comparable with the radial trap frequency $\omega_{x/y}$ in our system.

We then extract the cooling rate by measuring the atomic temperature after a variable time of of EIT cooling, as shown in Fig. 6(b). Here, we apply the optimal cooling parameters ($\Delta_c = \Delta_p = 2\pi \times 94.5$ MHz, $\Omega_c = 2\pi \times 5.06$ MHz, and $\Omega_p = 2\pi \times 2.0$ MHz) to the pair of coupling and probe beams. From an exponential fit to the experimental data, we deduce a $1/e$ cooling time constant of 2.1(3) ms and a steady-state temperature of around 5.9(2) μK.

V. DISCUSSION AND CONCLUSION

By applying EIT cooling optimized for the radial directions, we have successfully cooled the atom to a temperature of 5.7(1) μK. This is 2.5 times lower than the temperature of 14.7 μK typically achieved with conventional PGC. We note that our temperature measurement predominantly reveals the temperature along the radial direction due to the limitation of the "release and recapture" technique. Particularly, a Gaussian optical dipole trap typically has a much smaller spatial confinement in the radial direction than in the axial direction. Consequently, it is much easier for the atom to escape the trap in the radial direction during the release interval.

From the measured atomic temperature, we infer a mean phonon number of $\langle n_{x/y}\rangle = 1.18(5)$. This is higher than the theoretical value of 0.002 expected for our parameters from the rate equation described in [26]. Additionally, we also observe that the measured cooling time constant is about 10 times longer than the expected value of 0.2 ms estimated from the same theoretical work. These discrepancies are possibly due to unaccounted heating effects originating from scattering of the strong coupling beam which is red-detuned from the $|F=2, m_F=-2\rangle \leftrightarrow |F'=3, m_{F'}=-3\rangle$ cycling transition. In the absence of the EIT cooling, this scattering process alone would impose a lower limit on the energy reached to be in the order of $\sim\hbar\Gamma$, which is $\sim$100 μK in temperature. Furthermore, there is also heating due to the occasional repumping process. We speculate that the observed minimum temperature of 5.7 μK is a consequence of a steady state between the EIT cooling and these two scattering processes.

In addition, the cooling time would also be limited by the high probability (50%) of an atom in the state $|e\rangle$ of $5\,^2P_{3/2}$ $F'=2$ to decay into the $5\,^2S_{1/2}$ $F=1$ hyperfine level, which is decoupled from the pair of EIT cooling beams. Despite the use of a repump light to transfer the atom back to the $F=2$ state, this process introduces a delay as well as heating. In comparison, EIT cooling is 1.9 times slower than the conventional PGC, which has a typical $1/e$ cooling time constant of 1.1(1) ms [35].

Although prior work with EIT cooling has demonstrated approximate ground state occupation, the temperature of 5.7(1) μK achieved here is comparable to the 7 μK (or a mean phonon number of 0.78) obtained previously in a standing wave optical trap of [30] and an order of magnitude lower than the temperatures achieved in an ion trap [27]. Our demonstration could be extended to lower temperatures further by adding a second stage of EIT cooling that targets cooling along the axial direction with δ matched to the axial trap frequency spacing ω_z. Exploring strategies to mitigate heating caused by scattering in a multilevel atom could improve the cooling even further.

In conclusion, we have demonstrated electromagnetically induced transparency (EIT) cooling for a single neutral atom confined in a shallow optical dipole trap and have resolved the signature Fano profiles in the excitation spectrum due to a large solid angle for fluorescence collection. A final temperature of less than 6 μK has been reached with EIT cooling, a factor of 2 below the value obtained by polarization gradient cooling in the same system.

Technologically, the use of magnetic sublevels to realize the Λ scheme is convenient as it requires only a small frequency difference (on the order of MHz) between the pump and coupling fields, which allows simple frequency shifting from the same laser to provide both components. This cooling scheme therefore can diversify the spectrum of techniques for manipulation of atomic motion of ultracold atoms in optical tweezer arrays.

ACKNOWLEDGMENTS

We acknowledge the support of this work by the National Research Foundation, Prime Minister's office, and A*STAR under Project No. NRF2021-QEP2-01-P01/W21Qpd0101.

APPENDIX: OVERLAP OF MULTIPLE FANO RESONANCES

In our experiment, we assume to dominantly keep atoms only in one Λ system. However, different Λ configurations in the atomic level structure might be involved in the two-photon process as well. Apart from the $\Lambda^{(0)}$ system formed by $|g\rangle = |F=2, m_F=-2\rangle$, $|e\rangle = |F'=3, m_{F'}=-1\rangle$, and $|g'\rangle = |F=2, m_F=0\rangle$, there are the $\Lambda^{(1)}$ and $\Lambda^{(2)}$ systems with the respective $m_F, m_{F'}$ of the states increased by 1 and 2 (see Fig. 7).

The pair of probe and coupling fields drives each Λ system according to their respective dipole transition elements. By referring the two Rabi frequencies in $\Lambda^{(0)}$ as Ω_p for the $m_F = m_{F'}-1$ leg and Ω_c to the other one, the corresponding Rabi frequencies for $\Lambda^{(1)}$ and $\Lambda^{(2)}$ are $\Omega_p^{(1)} = \sqrt{3}\Omega_p$, $\Omega_c^{(1)} = \sqrt{3}\Omega_c$, $\Omega_p^{(2)} = \sqrt{6}\Omega_p$, and $\Omega_c^{(2)} = \Omega_c/\sqrt{6}$, respectively. Following Eq. (2), the spectral linewidth for these three Fano resonances are

$$\Gamma_+^{(0)} = \frac{\Gamma}{4\Delta_c^2+\Gamma^2}\left(\Omega_c^2+\Omega_p^2\right),$$
$$\Gamma_+^{(1)} = \frac{\Gamma}{4\Delta_c^2+\Gamma^2}\left(3\Omega_c^2+3\Omega_p^2\right),$$
$$\Gamma_+^{(2)} = \frac{\Gamma}{4\Delta_c^2+\Gamma^2}\left(6\Omega_c^2+\Omega_p^2/6\right). \tag{A1}$$

Furthermore, to simplify the analysis, we consider the same Rabi frequencies for the probe and coupling field in the $\Lambda^{(0)}$ configuration ($\Omega_p = \Omega_c = \Omega$), in line with the parameters in the Fano spectrum experiment. We then obtain $\Gamma_+^{(2)} = 3.08\Gamma_+^{(0)}$ and $\Gamma_+^{(1)} = 3\Gamma_+^{(0)}$, resulting in a Fano linewidth larger by a factor of 3. Additionally, aside from the difference in linewidths, the Fano peaks for the three Λ configurations will also exhibit distinct resonance shifts due to the difference in coupling strengths and also in Zeeman shifts. We expect the combination of these features contribute to the discrepancy of 4.7 between observed and expected Fano linewidth.

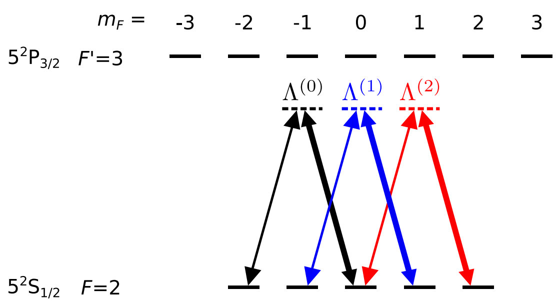

FIG. 7. Three possible Λ configurations involved in the two-photon process.

[1] S. Ebadi, T. T. Wang, H. Levine, A. Keesling, G. Semeghini, A. Omran, D. Bluvstein, R. Samajdar, H. Pichler, W. W. Ho, S. Choi, S. Sachdev, M. Greiner, V. Vuletić, and M. D. Lukin, Quantum phases of matter on a 256-atom programmable quantum simulator, Nature (London) **595**, 227 (2021).

[2] P. Scholl, M. Schuler, H. J. Williams, A. A. Eberharter, D. Barredo, K.-N. Schymik, V. Lienhard, L.-P. Henry, T. C. Lang, T. Lahaye, A. M. Läuchli, and A. Browaeys, Quantum simulation of 2d antiferromagnets with hundreds of rydberg atoms, Nature (London) **595**, 233 (2021).

[3] D. Bluvstein, H. Levine, G. Semeghini, T. T. Wang, S. Ebadi, M. Kalinowski, A. Keesling, N. Maskara, H. Pichler, M. Greiner, V. Vuleti, and M. D. Lukin, A quantum processor based on coherent transport of entangled atom arrays, Nature (London) **604**, 451 (2022).

[4] T. M. Graham, Y. Song, J. Scott, C. Poole, L. Phuttitarn, K. Jooya, P. Eichler, X. Jiang, A. Marra, B. Grinkemeyer, M. Kwon, M. Ebert, J. Cherek, M. T. Lichtman, M. Gillette, J. Gilbert, D. Bowman, T. Ballance, C. Campbell, E. D. Dahl *et al.*, Multi-qubit entanglement and algorithms on a neutral-atom quantum computer, Nature (London) **604**, 457 (2022).

[5] T. van Leent, M. Bock, R. Garthoff, K. Redeker, W. Zhang, T. Bauer, W. Rosenfeld, C. Becher, and H. Weinfurter, Long-distance distribution of atom-photon entanglement at telecom wavelength, Phys. Rev. Lett. **124**, 010510 (2020).

[6] P. Thomas, L. Ruscio, O. Morin, and G. Rempe, Efficient generation of entangled multiphoton graph states from a single atom, Nature (London) **608**, 677 (2022).

[7] Y.-S. Chin, M. Steiner, and C. Kurtsiefer, Quantifying the role of thermal motion in free-space light-atom interaction, Phys. Rev. A **95**, 043809 (2017).

[8] Y. Wang, X. Zhang, T. A. Corcovilos, A. Kumar, and D. S. Weiss, Coherent addressing of individual neutral atoms in a 3d optical lattice, Phys. Rev. Lett. **115**, 043003 (2015).

[9] C. H. Chow, B. L. Ng, and C. Kurtsiefer, Coherence of a dynamically decoupled single neutral atom, J. Opt. Soc. Am. B **38**, 621 (2021).

[10] A. M. Kaufman, B. J. Lester, C. M. Reynolds, M. L. Wall, M. Foss-Feig, K. R. A. Hazzard, A. M. Rey, and C. A. Regal, Two-particle quantum interference in tunnel-coupled optical tweezers, Science **345**, 306 (2014).

[11] M. O. Brown, S. R. Muleady, W. J. Dworschack, R. J. Lewis-Swan, A. M. Rey, O. Romero-Isart, and C. A. Regal, Time-of-flight quantum tomography of an atom in an optical tweezer, Nat. Phys. **19**, 569 (2023).

[12] C. J. Ballance, T. P. Harty, N. M. Linke, M. A. Sepiol, and D. M. Lucas, High-fidelity quantum logic gates using trapped-ion hyperfine qubits, Phys. Rev. Lett. **117**, 060504 (2016).

[13] R. T. Sutherland, Q. Yu, K. M. Beck, and H. Häffner, One- and two-qubit gate infidelities due to motional errors in trapped ions and electrons, Phys. Rev. A **105**, 022437 (2022).

[14] S. J. Evered, D. Bluvstein, M. Kalinowski, S. Ebadi, T. Manovitz, H. Zhou, S. H. Li, A. A. Geim, T. T. Wang, N. Maskara, H. Levine, G. Semeghini, M. Greiner, V. Vuleti, and M. D. Lukin, High-fidelity parallel entangling gates on a neutral
1 atom quantum computer, Nature (London) **622**, 268(2023).

[15] C. Monroe, D. M. Meekhof, B. E. King, S. R. Jefferts, W. M. Itano, D. J. Wineland, and P. Gould, Resolved-sideband raman cooling of a bound atom to the 3d zero-point energy, Phys. Rev. Lett. **75**, 4011 (1995).

[16] A. M. Kaufman, B. J. Lester, and C. A. Regal, Cooling a single atom in an optical tweezer to its quantum ground state, Phys. Rev. X **2**, 041014 (2012).

[17] J. D. Thompson, T. G. Tiecke, A. S. Zibrov, V. Vuletić, and M. D. Lukin, Coherence and raman sideband cooling of a single atom in an optical tweezer, Phys. Rev. Lett. **110**, 133001 (2013).

[18] B. Lounis and C. Cohen-Tannoudji, Coherent population trapping and fano profiles, J. Phys. II **2**, 579 (1992). 2

[19] G. Morigi, Cooling atomic motion with quantum interference, Phys. Rev. A **67**, 033402 (2003).

[20] A. T. Grier, I. Ferrier-Barbut, B. S. Rem, M. Delehaye, L. Khaykovich, F. Chevy, and C. Salomon, Λ-enhanced sub-doppler cooling of lithium atoms in D_1 gray molasses, Phys. Rev. A **87**, 063411 (2013).

[21] S. Rosi, A. Burchianti, S. Conclave, D. S. Naik, G. Roati, C. Fort, and F. Minardi, Λ-enhanced grey molasses on the D_2 transition of rubidium-87 atoms, Sci. Rep. **8**, 1301 (2018).

[22] M. O. Brown, T. Thiele, C. Kiehl, T.-W. Hsu, and C. A. Regal, Gray-molasses optical-tweezer loading: Controlling collisions for scaling atom-array assembly, Phys. Rev. X **9**, 011057 (2019).

[23] J. Ang'ong'a, C. Huang, J. P. Covey, and B. Gadway, Gray molasses cooling of ^{39}K atoms in optical tweezers, Phys. Rev. Res. **4**, 013240 (2022).

[24] G. Janik, W. Nagourney, and H. Dehmelt, Doppler-free optical spectroscopy on the ba$^+$ mono-ion oscillator, J. Opt. Soc. Am. B **2**, 1251 (1985).

[25] Y. Stalgies, I. Siemers, B. Appasamy, and P. E. Toschek, Light shift and fano resonances in a single cold ion, J. Opt. Soc. Am. B **15**, 2505 (1998).

[26] G. Morigi, J. Eschner, and C. H. Keitel, Ground state laser cooling using electromagnetically induced transparency, Phys. Rev. Lett. **85**, 4458 (2000).

[27] C. F. Roos, D. Leibfried, A. Mundt, F. Schmidt-Kaler, J. Eschner, and R. Blatt, Experimental demonstration of ground state laser cooling with electromagnetically induced transparency, Phys. Rev. Lett. **85**, 5547 (2000).

[28] R. Lechner, C. Maier, C. Hempel, P. Jurcevic, B. P. Lanyon, T. Monz, M. Brownnutt, R. Blatt, and C. F. Roos, Electromagnetically-induced-transparency ground-state cooling of long ion strings, Phys. Rev. A **93**, 053401 (2016).

[29] L. Feng, W. L. Tan, A. De, A. Menon, A. Chu, G. Pagano, and C. Monroe, Efficient ground-state cooling of large trapped-ion chains with an electromagnetically-induced-transparency tripod scheme, Phys. Rev. Lett. **125**, 053001 (2020).

[30] T. Kampschulte, W. Alt, S. Manz, M. Martinez-Dorantes, R. Reimann, S. Yoon, D. Meschede, M. Bienert, and G. Morigi, Electromagnetically-induced-transparency control of single-atom motion in an optical cavity, Phys. Rev. A **89**, 033404 (2014).

[31] E. Haller, J. Hudson, A. Kelly, D. A. Cotta, B. Peaudecerf, G. D. Bruce, and S. Kuhr, Single-atom imaging of fermions in a quantum-gas microscope, Nat. Phys. **11**, 738 (2015).

[32] U. Fano, Effects of configuration interaction on intensities and phase shifts, Phys. Rev. **124**, 1866 (1961).

[33] Y.-S. Chin, M. Steiner, and C. Kurtsiefer, Nonlinear photon-atom coupling with 4pi microscopy, Nat. Commun. **8**, 1200 (2017).

[34] C. Tuchendler, A. M. Lance, A. Browaeys, Y. R. P. Sortais, and P. Grangier, Energy distribution and cooling of a single atom in an optical tweezer, Phys. Rev. A **78**, 033425 (2008).

[35] Y.-S. Chin, M. Steiner, and C. Kurtsiefer, Polarization gradient cooling of single atoms in optical dipole traps, Phys. Rev. A **96**, 033406 (2017).

[36] J. Wu, R. Newell, M. Hausmann, D. J. Vieira, and X. Zhao, Loading dynamics of optical trap and parametric excitation resonances of trapped atoms, J. Appl. Phys. **100**, 054903 (2006).